International Journal of Research in Engineering and Science (IJRES)
ISSN (Online): 2320-9364, ISSN (Print): 2320-9356
www.ijres.org Volume 12 Issue 7 ǁ July 2024 ǁ PP. 183-194

Influences of Induced Magnetic Field and Velocity Slip on Hybrid Nano Fluid on a Stretching Wedge with Variable Heat Source

Ogunniyi, P. O., Ogboru K. O., Lawal M. M. and Okedoye, A. M.*
Department of Mathematics, Federal University of Petroleum Resources Effurun, Delta State, Nigeria.
**Corresponding Author: Okedoye.akindele@fupre.edu.ng*

Abstract
The analyses of hybrid Nano fluid have received tremendous attention because of its importance as coolants in electric vehicles, heat exchange systems, heat care, nuclear reactors, thermos-therapy, aerospace, naval structures, and in power plants. This work examines influences of velocity-slip and induced magnetic field on hybrid Nano fluid which is tangentially hyperbolic on a stretching wedge in the presence of variable heat source. Copper and aluminum oxides are the two nanoparticles used for this research, and the conventional fluid is water. The flow is modelled in form of partial differential equations which were reduced into ordinary forms before solving them using homotopy analysis approach. The influences of important parameters on induced magnetic, temperature, velocity, Nusselt number, and drag coefficient are examined. Findings are displayed on both tables and graphs which are agreed with the previous ones.

Keywords: *Heat Source: Hybrid Nano fluid: Induced Magnetic Field: Slip Effect: Stretching Wedge*

Date of Submission: 14-07-2024 Date of acceptance: 31-07-2024

I. INTRODUCTION

Numbers of decades ago have seen a rise in interest in studying boundary layer fluid flows associated uniform stretching sheet because of its numerous engineering and industrial uses. These include plastic film drawing, the production of glass fiber, production of paper, metal and polymer extrusion, hot rolling, wire drawing and metal spinning. The flow emanating from a sheet that is linearly stretched was initially examined by Crane [1]. Eventually, Carragher & Crane [2] added impact of thermal radiation to this problem. Magyari & Keller [3] studied the steady form of the flow over a sheet that stretches exponentially continuously with temperature distribution. Heat transfer of mixed convection was investigated with viscous heat from an exponentially extending surface by Partha et al. [4]. The work was expanded upon by Bidin and Nazar [5], who used numerical methods to address it while also looking at the influences of radiation on an exponentially stretching sheet. Ishak [6] studied the boundary layer of magneto hydrodynamic flow caused by a stretching sheet with importance on influence of the radiation while using the Keller box approach to solve the problem numerically. Elbashbeshy et al. [7] studied an unstable convection magneto hydrodynamic flow across a porous stretched sheet while considering impact radiation on the flow. Tufail et al. [8] researched on behaviours of heat source or sink on heat transfer associated with magneto hydrodynamic non-Newtonian flow across a porous stretched sheet.

Rasheed et al [9] reviewed applications of hybrid Nano fluid for solar and thermal appliances as sustainable and renewable suspensions. The report shows that increasing thermal properties of the fluid enhances the performances of the appliances. Shah et al [10] numerically studied impart of magneto hydrodynamic of a hybrid fluid in a permeable cylinder. The result of their work shows that the fluid is a good conductor because of retardation of the opposing Lorentz forces generated within the fluid. Tanzila, Nadeem, and Khan [11] numerically examined absorption and generation of heat within silver-copper oxide-water hybrid nanofluid. The study showed that heat transfer is lower in just nanofluid than the hybrid form. Muhammad *et al* [12] used runge-kutta method to investigate a stagnation point of a Hybrid Nanofluid on a Stretching plate. Sreedevi, Sudarsana Reddy & Chamkha [13] analyzed heat and mass radiating effects of multiple walls carbon nanotube and silver hybrid nanofluid of water over a stretching plate. The research shows, among other, that boundary layer thickens by intensifying thickness of the nano particles volumes. Alnahdi and Gul [14] explored movement of hybrid nanofluid over a slippery sheet. Their result shows that the fluid hybridization enhances thermal properties of the fluid.

One well-understood phenomenon pertaining to fluids' non-adherence to surfaces is the slip boundary condition. Fluids with slip properties are helpful in several areas, such as internal cavities and prosthetic heart valve cleaning. In this case, the determining coefficient is the Kundsen number. This measures the molecular mean-free-path to characteristic length. The fundamentals of continuum mechanics are in line when there is no discernible slip between the fluid and the surface at very small Knudsen numbers. Beavers & Joseph [15] devised a boundary slip condition. The effects of the velocity-slip on magneto hydrodynamic flow and heat transmission across a porous stretched membrane were quantitatively studied by Afify et al. [16].

However, the no-slip condition, which is the presumption that a liquid clings to a solid barrier. One of the fundamental assumptions of the Navier-Stokes theory is the no-slip boundary condition. On the stretching boundary, partial velocity slip happens if the fluid is particulate, as in the case of suspensions, emulsions, polymer solutions, and foams.

Using the Adomian decomposition scheme, Gbadeyan, Abubakar, and Oyekunle [17] examined a spiral channel's effects of Navier slip on a steady incompressible fluid flow. The findings showed that a higher slip parameter improves heat transfer at wavy walls while decreasing it at flat walls. Aziz, Siddique, and Aziz [18] conducted a numerical analysis of a continuous boundary layer slip flow via a permeable plate positioned deeply within a penetrable medium. The study's conclusion showed that while the medium's porosity increases fluid velocity, it also opposes the fluid's thermal boundary layer. Research on the free convection exothermic slip fluid flow was conducted by Hamza [19]. Using the perturbation series approach, he was able to solve the nonlinear equations that he ran across. The project authorized that the fluid flow largely dependent on the slip. Numerous other scholars have recently [20–22], among others, examined flow problems while considering slip conditions at the boundary because of its significant technological uses in the polishing of prosthetic interior cavities and heart valves.

The term "induced magnetic field" (IMF) refers to the extra magnetic field which is produced on fluid that conducts electrically when an external magnetic field is present. This is brought about by a greater magnetic Reynolds number. Glass manufacturing, magneto hydrodynamics generators and geophysics are a few applications for IMF. The IMF and blood flow work together to provide vital support for blood pumps, heart disease therapy, and numerous biomedical uses. Kumari et al. [23] examined the influences of IMF and heat sources/sink of fluid flow which conducts electrically on an elongating sheet. Subsequently, Ali and associates [24] reviewed the MHD flow through an expanding sheet with an induced magnetic field.

Hayat, Asad and Alsaedi [25] examined variable heat source in a stretched cylindrical flow in the presence of heat radiation. The findings show that curvature parameter enhances the flow velocity, but it retards the fluid temperature. Konda, Madhusudhana, Konijeti and Dasore [26] investigated non-uniform heat and magnetic field effects on Williamson nanofluid in a permeable medium. The outcomes show that Eckert number enhances velocity of the flow while it slows down the fluid temperature. Manyi et al [27] researched on variable heat source influence over a stretching sheet on radiating Eyring Powell fluid. The result shows among other that thermal parameter retards velocity of the flow and its temperature. Rawat and others [28] worked on importance of variable heat between two rotating but parallel plates on hybrid fluid in a Darcy-Forchheimer permeable medium. The investigation reveals that heat relaxation parameter retards transmission of the heat between the plates. Mehmood, Hussain and Sagheer [29] numerically examined impacts of variable heat source on convective magneto-nanofluid flow by shooting method. The outcome obtained is that fluid velocity reduces and fluid temperature increase as mass and heat parameter reduces.

The heat and mass transfer analysis of the flow over a stretching sheet has been the subject of extensive research recently due to its vital applications in the pharmaceutical engineering, metallurgy, and space technology industries, including food processing technology, various hospital treatments, and polymer production, Okedoye and Ogunniyi [30] worked on binary chemical reaction and mass transfer of boundary layer flow through a moving plate. As a result, the work of Mohamed and Ahmed [31] is expanded to incorporate the effects of induced magnetic field and velocity-slip in the presence of variable heat source of the considered hybrid fluid on a stretching wedge. Therefore, the results are contrasted with previous findings as well as those of Mohamed and Ahmed [31]

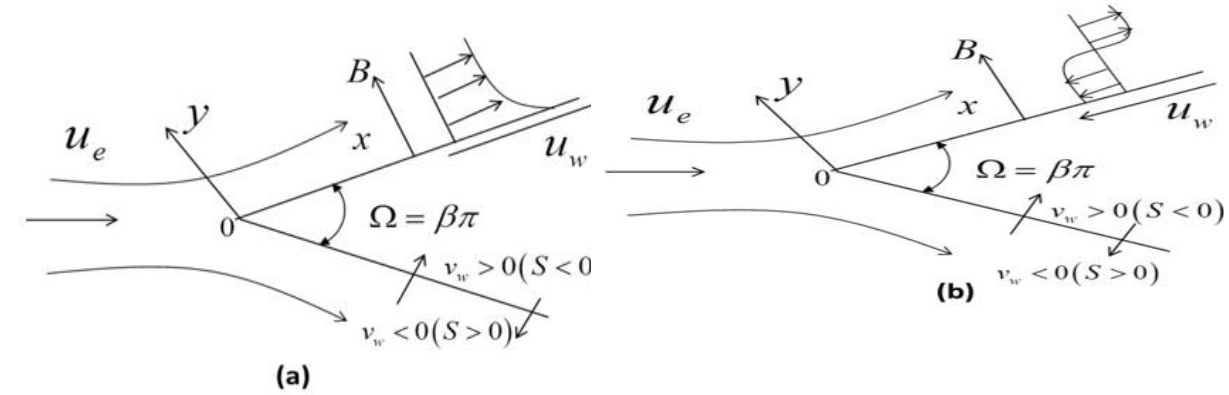

Fig. 1(a, b): Schematic Diagram of the Flow

II. PROBLEM FORMULATION

Let us suppose a steady, convective flow across a stretching wedge that is laminar, and hydro magnetic coupled heat and mass transfer. The fluid is taken to be Newtonian, and conducts electrically. Its temperature as well as induced magnetic field-driven fluctuations are restricted to the fluid density. The momentum equation makes the assumption that the effects of buoyancy and density variation are minimal (Boussinesq approximation). Furthermore, no applied electric field is present, and Joule heating and all of the Hall effects are disregarded. It is assumed that the induced magnetic field influenced the fluid flow properties. Let the y-axis be normal to the plate and the x-axis to be taken along its direction. If u is the velocity-component along x-axis, v is the velocity-component along the y-axis, T is the fluid temperature, and Bi (i = 1, 2) is the induced magnetic field; then, by boundary-layer as well as Boussinesq approximation, the controlling equations of the flow can be written thus, Mohamed and Ahmed [31]:

$$u_x + u_y = 0, \tag{1}$$

$$B1_x + B2_y = 0, \tag{2}$$

$$uu_x + vu_y = \frac{\mu_e}{4\pi\rho_{hnf}}\left(B_1 B1_x + B_2 B1_y - B_e\frac{dB_e}{dx}\right) + u_e\frac{du_e}{dx} \pm \frac{\mu_{hnf}}{\rho_{hnf}}\left(\left(\frac{1+\gamma}{\gamma}\right) + \sqrt{2n\Gamma}u_y\right)u_{yy} + \frac{g\beta(T-T_\infty)}{\rho_{hnf}} \tag{3}$$

$$uB1_x + vB1_y = B_1 u_x + B_2 u_y + \mu_0\frac{\partial^2 B_1}{\partial y^2}, \tag{4}$$

$$uT_x + vT_y = \frac{k_{hnf}}{(\rho c_p)_{hnf}}T_{yy} + \frac{\mu_{hnf}}{(c_p\rho)_{hnf}}(u_y)^2 + \frac{1}{\gamma}\frac{\mu_{hnf}}{(c_p\rho)_{hnf}}(u_y)^2 + \frac{1}{\sigma(c_p\rho)_{hnf}}(B1_y)^2 + \frac{k_{hnf}}{(\rho c_p)_{hnf}}\frac{\partial q'''}{\partial y} \tag{5}$$

The amount of heat produced is:

$$q''' = \left(\frac{k_{hnf}u_w(x)}{xv_f}\right)\left[\frac{A^*(T_w - T_\infty)}{bx}u + Q_0(T - T_\infty)\right] \tag{6}$$

Where(Q_0, A^*) denotes the temperature and space The coefficient for the heat source or sink that depends on something. In addition, when A is greater than 0 and Q_0 is greater than 0, it means heat is being generated internally. On the other hand, when A is less than 0 and Q_0 is less than 0, it means heat is being absorbed internally. Now, (5) and (6) reduce to:

$$uT_x + vT_y = \frac{(B1_y)^2}{\sigma(c_p\rho)_{hnf}} + \frac{\mu_{hnf}}{(c_p\rho)_{hnf}}\left(1 + \frac{1}{\gamma}\right)(u_y)^2 + \frac{k_{hnf}}{(\rho c_p)_{hnf}}\left(T_{yy} - \frac{u_w(x)}{xv_f}\left[\frac{A^*(T_w - T_\infty)}{bx}u + Q_0(T - T_\infty)\right]\right) \tag{7}$$

The conditions at the wedge's boundary are given by:

$$u = N\left(\tfrac{1}{\gamma} + 1\right)u_y + u_w(x), v = v_w, B_2 = B1_y = 0, -\kappa_{hnf}T_y = q_f \text{ when } y = 0$$
$$u \to U_\infty, T \to T_\infty, B_0 \to B_1, \text{ when } y \to \infty \tag{8}$$

Where, here and anywhere else B_y is magnetic component in y-direction, B_x is magnetic component along x-directions, $u_w(x) = cx$ is velocity of the wedge while a & c are positive constants, μ_0 is magnetic permeability, $u_e(x) = ax$ is velocity of the fluid beyond the wedge's boundary, $B_e(x) = B_0(x/L)$ is wedge's boundary's magnetic field, B_0 is upstream uniform magnetic field, η_0 is magnetic diffusivity, Q_0 is heat source, N is velocity-slip, L is length of the wedge, T_∞ is temperature away from the wedge, q_r is heat flux, k is thermal conductivity, μ is dynamics viscosity, ρ is density, ρc_p is heat capacity, σ is electrical conductivity, hnf is hybrid nano fluid, nf is nano fluid, f is fluid, $f(\eta)$ is fluid velocity, $g(\eta)$ is induced magnetic field, $\theta(\eta)$ is fluid temperature, T_w is wedge's temperature at its boundary, γ is Newtonian parameter, Γ is tangential hyperbolic parameter, n is fluid rotation parameter, g is gravitational acceleration, and h is the wedge's heat transfer coefficient.

2.2 **Rate of Heat and Mass Transfer at the wall**

According to Mohamed and Ahmed [31], the wedge's wall heat (Skin friction, Cf) and Nano mass transfer (Nusselt number, Nu) rates are defined as:

$$c_f = \frac{\tau_w}{U_w^2 \rho_{nf}}, Nu = \frac{-x q_w}{(T_\infty - T_w) k_{nf}} \tag{9}$$

Note that τ_w (wall shear stress) & q_w(heat transfer) are given as

$$\tau_w = \left[\left(\frac{P_y}{\sqrt{2\pi_c}} + \mu_B\right) u_y\right]_{y=0} \quad q_w = \left[-k_{nf} T_y\right]_{y=0} \tag{10}$$

III. METHOD OF SOLUTION

The stream function $\psi_{u,B}$ which stands for both magnetic field and velocity, and satisfies (1) and (2) is:

$$\psi_u = \sqrt{x U_w \nu_{nf}} f(\eta), \quad \psi_B = \sqrt{x B_e \nu_{nf}} g(\eta), \quad \eta = \sqrt{\frac{U_w}{\nu x}} y, \tag{11}$$

where $u = \psi_{u_y}, v = -\psi_{u_x}, \; u = \psi_{B_y}, v = -\psi_{B_x}$

Temperature is given in the dimensionless form as

$$T = (T_w - T_\infty)\theta(\eta) + T_\infty \tag{12}$$

But B_e and $U_w$are defined as:

$$(B_e, u_w) = \left(\frac{x B_0}{L}, cx\right) \tag{13}$$

Then (11) and (13) become

$$\psi_u = \sqrt{c \nu_{nf}} x f, \quad \psi_B = \sqrt{\frac{B_0 \nu_{nf}}{L}} x g(\eta), \quad \eta = \sqrt{\frac{c}{\nu_{nf}}} y \tag{14}$$

Hence,

$$B_1 = \sqrt{\frac{c B_0}{L}} x g'(\eta), B_2 = -\sqrt{\frac{\nu_{nf} B_0}{L}} g(\eta), u = xcf'(\eta), v = -\sqrt{c \nu_{nf}} f(\eta) \tag{15}$$

The transformed forms of (3), (4) and (9) by using (14) - (19) are:

$$A^2 N_1 - N_4 Pr f_\eta + H\left((g_\eta)^2 - g(\eta) g_{\eta\eta} - 1\right) + N_1 f(\eta) f_{\eta\eta} + N_4\left(1 + \tfrac{1}{\gamma}\right) f_{\eta\eta\eta} + Grt\,\theta(\eta) - \tfrac{N_4 N_1}{\gamma} W_e (f_{\eta\eta}) f_{\eta\eta\eta} - N_1 (f_\eta)^2 = 0 \tag{16}$$

$$\frac{1}{Pm} g_{\eta\eta\eta} + f(\eta) g_{\eta\eta} - g(\eta) f_{\eta\eta} = 0 \tag{17}$$

$$\frac{N_3}{Pr}\left(1 + \frac{4R_d}{3}\right)\theta_{\eta\eta} + \frac{HEc}{N_5 Pm}(g_{\eta\eta})^2 - N_2 f(\eta)\theta_\eta + \frac{N_2}{Pr}\left(\alpha f_\eta + \beta\theta(\eta)\right) + EcN_3\left(1 + \frac{1}{\gamma}\right)(f_{\eta\eta})^2 = 0 \tag{18}$$

And corresponding boundary conditions (10) are:

$$\begin{aligned} &f(0) = S, f'(0) = \left(\frac{1}{\gamma} + 1\right)\lambda_1 f_{yy} + 1, \\ &g''(\eta) = 0 = g(\eta), \theta_y = \omega(\theta(0) - 1) \\ &f_\eta \to A, g_\eta \to 1, \theta(\eta) \to 0 \;\; \text{as}\; \eta \to \infty \end{aligned} \tag{19}$$

With flow parameters:

$$A=\frac{a}{c},\lambda 1=\sqrt{\frac{c}{\nu_{nf}}}N,Rd=\frac{4\sigma T_{\infty}^{3}}{3k_{s}},Pm=\sigma\mu_{nf}\nu_{nf},Pr=\frac{\left(\mu c_{p}\right)_{nf}}{k_{nf}},$$
$$Grt=\frac{g\beta_{T}(T_{w}-T_{\infty})}{\rho_{nf}c^{2}x},Ec(T_{w}-T_{\infty})=\frac{c^{2}x^{2}}{(c_{p})_{nf}},H=\frac{\mu_{e}B_{0}^{2}}{(cL)^{2}\rho_{nf}} \quad (20)$$

Where A is the stretching parameter, $\lambda 1$is velocity-slip, Rd is thermal radiation, Pm is inverse of induced Prandtl number, Pr is Prandtl number, Grt is Grashof number, Ec is Eckert number, H is magnetic field,

$$N1=\frac{\rho_{hnf}}{\rho_{f}},N2=\frac{(\rho cp)_{hnf}}{(\rho cp)_{f}},N3=\frac{k_{hnf}}{k_{f}},N4=\frac{\mu_{hnf}}{\mu_{f}},N5=\frac{\sigma_{hnf}}{\sigma_{f}}.$$

3.2 **The Skin-Friction and Heat Transfer at the wall**

The interesting quantities are local skin-friction c_{fx} and local Nusselt number Nu_{x}. These are defined as:

$$c_{f}=(Re_{x})^{-1/2}\left[\frac{1}{\gamma}W\left(f_{\eta\eta}\right)^{2}+\left(\frac{\gamma+1}{\gamma}\right)f_{\eta\eta}\right]_{\eta=0},Nu=-N_{3}(Re_{x})^{1/2}(Ra+1)\left[\theta_{\eta}\right]_{\eta=0} \quad (21)$$

where, local Reynolds number, $Re_{x}=u_{w}x/\nu_{nf}$

Thermophysical Features

Table 1 presents the thermophysical characteristics of Al_2O_3, Cu, and Water, as reported by Ogunniyi et al [32]. Thermophysical property assessment models for the nanofluid are displayed in **Table 2**, and hybrid nanofluid thermophysical property equations are displayed in **Table 3**. ϕ_1 represents the Al_2O_3 volume fraction, whereas ϕ_2 represents the Cu volume percentage. When dealing with a single nanofluid, $\phi_1 = \phi_2 = 0$, when appropriate, subscripts f, s1, and s2 stand for fluid, Cu-solid component, and Al_2O_3- solid component, respectively.

Table 1: The properties of Cu, Al_2O_3 and H_2O

Properties	Al_2O_3	Cu	H_2O
C_p	765	385	4179
ρ	3970	8933	997.1
κ	40	4×10^{2}	613×10^{-3}
σ	369×10^{5}	596×10^{5}	5×10^{-2}

Table 2: The Models the Nano fluid:

Properties	The Nanofluid
$\rho\backslash Kgm^{-3}$	$\rho_{hnf}=(1-\phi_{2})(1-\phi_{1})+\frac{1}{\rho_{f}}\left(\phi_{2}\rho_{s_{2}}+(1-\phi_{2})\rho_{s_{1}}\phi_{1}\right)$
$\rho C_{p}\backslash Jm^{-3}K^{-1}$	$\left(\rho C_{p}\right)_{nf}=\left(\left(\rho C_{p}\right)_{s}-\left(\rho C_{p}\right)_{f}\right)\phi+\left(\rho C_{p}\right)_{f}$
μ	$\mu_{nf}=(1-\phi)^{-\frac{25}{10}}\mu_{f}$
$\kappa\backslash Wm^{-1}K^{-1}$	$k_{nf}=\left(\frac{k_{s}-(1-n)\left(k_{f}+(k_{f}-k_{s})\phi\right)k_{f}}{k_{s}+k_{f}(n-1)-(k_{s}-k_{f})\phi}\right)k_{f}$
$\sigma\backslash Sm^{-1}$	$\sigma_{nf}=\frac{\sigma_{s}+\left((\sigma_{f}-\sigma_{s})\phi-\sigma_{f}\right)(1-n)}{\sigma_{s}+(\sigma_{f}-\sigma_{s})\phi+\sigma_{f}(n-1)}\sigma_{f}$

Table 3: The Models for the hybrid Nano Fluid:

Property	The Hybrid Nano Fluid
Density	$\rho_{hnf}=\frac{\phi_{2}\rho_{s_{2}}}{\rho_{f}}-(\phi_{2}-1)\left[(1-\phi_{1})+\frac{\rho_{s_{1}}\phi_{1}}{\rho_{f}}\right]$
Heat capacity	$\left(\rho C_{p}\right)_{hnf}=\left(\frac{\left(\rho C_{p}\right)_{s_{2}}\phi_{2}}{\left(\rho C_{p}\right)_{f}}-\left[\frac{\left(\rho C_{p}\right)_{s_{1}}\phi_{1}}{\left(\rho C_{p}\right)_{f}}+(1-\phi_{1})\right](\phi_{2}-1)\right)\left(\rho C_{p}\right)_{f}$
Viscosity	$\mu_{hnf}=\mu_{f}[1-\phi_{1}-\phi_{2}+\phi_{1}\phi_{2}]^{-2.5}$
Thermal conductivity	$\kappa_{hnf}=\left(\frac{\kappa_{s_{2}}+2\kappa_{f}+2\phi_{2}\left(\kappa_{s_{2}}-\kappa_{f}\right)}{\kappa_{s_{2}}+2\kappa_{f}+\phi_{2}\left(\kappa_{f}-\kappa_{s_{2}}\right)}\times\frac{\kappa_{s_{1}}+2\kappa_{f}+2\phi_{2}\left(\kappa_{s_{1}}-\kappa_{f}\right)}{\kappa_{s_{1}}+2\kappa_{f}+\phi_{1}\left(\kappa_{f}-\kappa_{s_{1}}\right)}\right)\kappa_{f}$
Electrical conductivity	$\frac{\sigma_{hnf}}{\sigma_{f}}=\left[1+\frac{\sigma_{s_{2}}\phi_{s_{2}}-3\left(\phi\sigma_{f}-\sigma_{s_{1}}\phi_{s_{1}}\right)}{2\sigma_{f}+\phi\sigma_{f}-\sigma_{s_{1}}\left(\phi_{s_{1}}-1\right)-\sigma_{s_{2}}\left(\phi_{s_{2}}-1\right)}\right]$

3.3 **Numerical Computation**

The solution procedure is carried out by homotopy analysis technique. It involves obtaining base functions as a solution set $\{f(\eta),\theta(\eta),g(\eta)\}$ for the considered fluid flow model, and defined (Liao [33, 34]) as:

$$g(\eta)=\sum_{n=0}^{\infty}\sum_{k=0}^{\infty}b_{k,n}^{*}e^{-n\eta}\eta^{k};\ f(\eta)=\sum_{n=0}^{\infty}\sum_{k=0}^{\infty}a_{k,n}^{*}e^{-n\eta}\eta^{k};\ \theta(\eta)=\sum_{n=0}^{\infty}\sum_{k=0}^{\infty}c_{k,n}^{*}e^{-n\eta}\eta^{k} \tag{22}$$

Where$c_{k,n}^{*}$, $b_{k,n}^{*}$,$a_{k,n}^{*}$ are constants.

By the solution procedure, initial approximations for the boundary conditions are:

$$f_0(\eta)=\frac{1}{1+\lambda_1}-\frac{1}{1+\lambda_1}e^{-\eta}+1,\theta_0(\eta)=\frac{\beta_i}{N_3}(e^{-\eta}-1),g_0(\eta)=e^{-\eta} \tag{23}$$

The auxiliary linear operators L_f, L_g and $L\theta$ are:

$$L_f(f)-f'''(\eta)+f'(\eta)=L_g(f)-g'''(\eta)+g(\eta)=L_\theta(f)-\theta''(\eta)+\theta(\eta)=0 \tag{24}$$

The (3) is satisfied by:

$$L_f(c_3e^{-\eta}+c_2e^{\eta}+c_1)=L_\theta(c_7e^{\eta}+c_8e^{-\eta})=L_g(c_4+c_5e^{\eta}+c_6e^{-\eta})=0 \tag{25}$$

The Zeroth-order deformation for the equations is

$$\left.\begin{aligned}(1-p)[f_0(\eta)-f(\eta;p)]L_f&=-p\hbar N_f[f,\theta,g]\\(1-p)[\theta_0(\eta)-\theta(\eta;p)]L_\theta&=-p\hbar N_\theta[f,\theta,g]\\(1-p)[g_0(\eta)-g(\eta;p)]L_g&=-p\hbar N_g[f,\theta,g]\end{aligned}\right\} \tag{26}$$

Where,$\hbar$ is auxiliary parameter and p is embedding parameter.

$$\left.\begin{aligned}N_f[f,g,\theta]&=\frac{N_4}{N_1}\left(\frac{1}{\gamma}Wf_{\eta\eta}+\left(\frac{\gamma+1}{\gamma}\right)\right)f_{\eta\eta\eta}+f_{\eta\eta}f_{\eta}\\&A^2-\left(g_{\eta\eta}g_{\eta}-\left(g_{\eta}\right)^2+1\right)H^2-\left(f_{\eta}\right)^2+Gr\theta\\N_g[f,g,\theta]&=g_{\eta\eta\eta}-P_m\left(gf_{\eta}-fg_{\eta\eta}\right)\end{aligned}\right\}$$

$$\left.\begin{aligned}N_\theta[f,g,\theta]=&\frac{1}{\Pr}\left(N_3+\frac{4}{3}N_2Rd\right)\theta_{\eta\eta}+\frac{1}{\Pr}\left(ae^{-\eta}+b\theta\right)\\&+N_2f\theta_{\eta}+Ec\left(\left(1+\frac{1}{\gamma}\right)\left(f_{\eta\eta}\right)^2+\frac{H}{Pm}\left(g_{\eta\eta}\right)^2\right)\end{aligned}\right\} \tag{27}$$

With the boundary conditions given by:

$$\left.\begin{aligned}f'(0)=U_{slip}f''(0)+A,f(0)=g(0)=g''(0)=0,\\f'(0)=1=g'(\infty);\ \ \theta'(0)=\frac{\beta_i}{N_3}(\theta-1),f'(\infty)=\theta(\infty)=0;\end{aligned}\right\} \tag{28}$$

Mth-order Deformation Equation

If $p=0$ in (5) while differentiating m-times wrt p, and dividing by m! The higher-order deformation equations reduce to:

$$[\chi_mf_{m-1}-f_m]L_f=-\hbar_fR_m^f;\ \ [g_m-\chi_mg_{m-1}]L_g=\hbar_gR_m^g;\ \ (\theta_m-\chi_m\theta_{m-1})L_\theta=\hbar_\theta R_m^\theta \tag{30}$$

With boundary conditions:

$$\left.\begin{aligned}f_m'(0)=\left(\frac{1+\gamma}{\gamma}\right)\lambda_1f_m''(0)+1;\ f_m(0)=S;\ g_m'(\infty)=1\\f_m'(\infty)=A,\omega\theta_m'(0)+1-\theta_m(0)=g_m(0)=g_m''(0)=\theta_m=0\end{aligned}\right\} \tag{31}$$

Where

$$\theta_m(\eta)=\frac{1}{m!}\frac{\partial^m\theta(\eta,p)}{\partial\eta^m};\ \ f_m(\eta)=\frac{1}{m!}\frac{\partial^mf(\eta,p)}{\partial\eta^m};\ g_m(\eta)=\frac{1}{m!}\frac{\partial^mg(\eta,p)}{\partial\eta^m} \tag{31}$$

$$\left.\begin{aligned}R_m^f(\eta)=A^2+&\left(\left(\frac{1}{\gamma}+1\right)f_{m-1}'''+\frac{1}{\gamma}W\sum_{n=1}^{m-1}f_n''f_{m-1-n}'''\right)\frac{N_4}{N_1}-\sum_{n=1}^{m-1}f_n'f_{m-1-n}'\\&+\sum_{n=1}^{m-1}f_nf_{m-1-n}''+\left(\sum_{n=1}^{m-1}f_n'g_{m-1-n}'-\sum_{n=1}^{m-1}g_{m-1-n}'g_n''-1\right)\mathrm{H}+Gr\theta_{m-1}\\R_m^g(\eta)=P_m&\left(\sum_{n=1}^{m-1}f_{m-1-n}g_n''-\sum_{n=1}^{m-1}f_n''g_{m-1-n}\right)+g_{m-1}'''\end{aligned}\right\}$$

$$R_m^{\theta}(\eta) = Ec\left(\left(\frac{1}{\gamma}+1\right)\sum_{n=1}^{m-1} f''_{m-1-n}f''_n + \frac{H}{Pm}\sum_{n=1}^{m-1} g''_{m-1-n}g''_n\right) + \beta\theta_{m-1} \\ N_2\sum_{n=0}^{m-1}\theta'_n f_{m-1-n} + \frac{1}{Pr\left(\left(N_3+\frac{4}{3}N_2Rd\right)\theta''_{m-1}+\alpha f'_{m-1}\right)}\Bigg\} \quad (32)$$

And$\chi_m = 1$ (for $1 \le m$) or 0 (for $1 \ge m$)
When $p = 1$ and $p = 0$, we have:

$$\left.\begin{array}{l} f(0) - f_0(\eta) = f(1) - f(\eta) = 0 \\ g(0) - g_0(\eta) = g(1) - g(\eta) = 0 \\ \theta(0) - \theta_0(\eta) = \theta(1) - \theta(\eta) = 0 \end{array}\right\} \quad (33)$$

As$p$varies value 0to1. The$f(\eta,p)$,$\theta(\eta,p)$, $g(\eta,p)$also vary from initial functions $f_0(\eta)$, $\theta_0(\eta)$, $g_0(\eta)$to final ones $f(\eta)$,$\theta(\eta)$ $g(\eta)$respectively.
By Taylor's series expansion, it reduces to:

$$f - f_0(\eta) = \sum_{m=1}^{\infty} f_m(\eta)p^n\,,\ g - g_0(\eta) = \sum_{m=1}^{\infty} g_m(\eta)p^n\,,\ \theta - \theta_0(\eta) = \sum_{m=1}^{\infty}\theta_m(\eta)p^n\Big|_{p=0} \\ \left(f_m = \frac{1}{m!}\frac{\partial^m}{\partial\eta^m}f(\eta,p), \theta_m = \frac{1}{m!}\frac{\partial^m}{\partial\eta^m}\theta(\eta,p), g_m = \frac{1}{m!}\frac{\partial^m}{\partial\eta^m}g(\eta,p)\ \Big|\right)_{p=0} \quad (34)$$

The series (12) converge at $p = 1$ with appropriate value of the auxiliary parameter
Hence, the general solutions to the equations are:

$$\left.\begin{array}{l} f_m(\eta) = f_m^*(\eta) + c_1^m + c_2^m e^{\eta} + c_3^m e^{-\eta}, \\ \theta_m(\eta) = \theta_m^*(\eta) + c_7^m e^{\eta} + c_8^m e^{-\eta}, \\ g_m(\eta) = g_m^*(\eta) + c_4^m + c_5^m e^{\eta} + c_6^m e^{-\eta} \end{array}\right\} \quad (35)$$

Subjected to conditions:

$$\theta_m(\eta) = \theta_m^*(\eta) + c_7^m e^{\eta} + c_8^m e^{-\eta}, c_3^m = c_5^m = cc_7^m = g_m^*(0)_6^m = 0, c_1^m = -c_2^m - f_m^*(0),$$

$$c_4^m = 1 + \frac{f_m^{*\prime}(0) - \lambda_1 f_m^{*\prime\prime}(0)}{A+\lambda_1}, c_7^m = g_m^*(0), c_8^m = \frac{\omega\left(\theta_m^*(0) - \theta^*(0)\right)}{N_3}$$

where, $C_i; i = 1,2,\dots,8$ are constants.

RESULT AND DISCUSSION

The findings of the current work agreed to those obtained by Mohamed & Ahmed [31], Ali et al [24], Ishak et al [35], and Mahapatra & Gupta [36] if variable heat source or heat sink and magnetic thermal buoyancy ($Grt = 0$) are negligible. The compared results, which are displayed in Table 4, are in excellent agreement with one another for the other Pr numbers. Unlike the numerical solution previously described, the Prandtl number utilized in this case corresponds to plasma ($Pr = 0.7$Table 4: Drag coefficient $Cf_x\,Re_x^{1/2}$for different A values when $H = W = n = \alpha = w = \phi = 0$

A	Current Study	Mohamed & Ahmed [31]	Ali et al [24]	Ishak et al [35]	Mahapatra & Gupta [36]
0.1	-0.9693861	-0.969386	-0.9694	-0.9694	-0.9694
0.2	-0.9181070	-0.918107	-0.9181	-0.9181	-0.9181
0.5	-0.6672636	-0.667263	-0.6673	-0.6673	-0.6673
2.0	2.0175028	2.017500	2.0175	2.0175	2.0175
3.0	4.7292823	4.729280	4.7293	4.7294	4.7293

Table 5: The Rate of heat transfer at the wall of the stretching wedge for $\lambda 1 = 0.3, Grt = 0.05, \beta = 0.4, Ec = 0.2, \alpha = 0.2$

A	$\theta'(0)$	$f''(0)$
$A = 0.3$	0.108396	−0.569814
$A = 0.6$	0.037224	−0.461357
$A = 1.2$	−0.064989	0.191149
$\lambda 1 = 0.5$	0.117025	−0.475296
$\lambda 1 = 1.0$	0.131884	−0.338050

A	$\theta'(0)$	$f''(0)$
$\lambda 1 = 1.6$	0.142897	−0.252236
$Grt = -0.04$	0.181468	−0.649739
$Grt = 0.15$	0.067032	−0.497820
$Grt = 0.40$	0.010696	−0.346968
$\beta = -0.6$	−0.527427	−0.594349
$\beta = 0.0$	−0.207029	−0.582424
$\beta = 0.2$	−0.086857	−0.577797
$Ec = 0.8$	0.133505	−0.569306
$Ec = 1.6$	0.166850	−0.568631
$Ec = 3.2$	0.233084	−0.567291
$\alpha = -0.4$	−0.555705	−0.596498
$\alpha = 0.2$	0.108396	−0.569814
$\alpha = 0.4$	0.305804	−0.560811

This study examines the effects of fluid regulating parameters of the hybrid nanofluid on the stretching wedge. Drag coefficient and Nusselt number solutions validate the semi-analytical solution derived by the homotopy analysis approach. The findings are displayed in Fig. 2-15, and on tables 4 and 5.

Effects of Parameters Variation on Velocity Field

The non-negative effect of the stretching parameter on the velocity of the fluid f′(η) is illustrated in Fig. 2. The expansion of f′(η) occurs as the stretching parameter is strengthened. The velocity profiles for the nano fluid and hybrid nano fluid flow situations coincide when A=1. Furthermore, it is noted that in this instance, the fluid and the wedge's surface move at the same speed when velocity = 1 and acceleration = 0. Additionally, it is noted that the profile of the fluid velocity exhibits an increasing function when the stretching parameter A > 1, but the opposite trend is seen when A < 1. The fluid velocity f ′(η) is shown in Fig. 3 as a non-negative function of the magnetic parameter (H). An enhancement of the magnetic parameter causes f′(η) to expand. The effect of Weissenberg number (W) on fluid velocity is shown in Fig, 4. It is found that a surge in the W reduces the hydrodynamic boundary layer's strength and velocity. Fig. 5 illustrates the behavior of velocity-slip parameter on the fluid velocity. Increasing the parameter retards the fluid velocity along the boundary of the wedge. The influence of thermal Grashof number is depicted in Fig. 6. The velocity of the fluid is enhanced by escalating the Grashof parameter.

Effects of Parameters Variation on Induced Magnetic Field

The induced magnetic field, g(η), is influenced by the stretching parameter (A) as demonstrated in Fig. 7. It shows that, in both the nano fluid and hybrid nano fluid scenarios, the generated magnetic field profile decreases as the parameter increases. Also increasing values of magnetic field (H) amplified the induced magnetic field, g(η), as shown in Fig. 8. Fig. 9 illustrates the influence of inverse of the magnetic Prandtl number (Pm) on g(η). Rising Pm values cause decrease in the strength of the induced magnetic field, g(η).

Effects of Parameters Variation on Temperature Field

In Fig. 10, the rising A-value indicates a drop in fluid's temperature. Notably, when the stretching parameter is increased, the temperature profiles in the case of nanofluid flow are lower than those in the hybrid nanofluid flow.

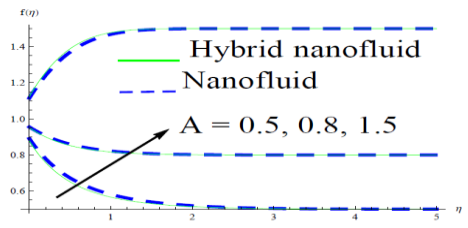

Fig. 2: Impact of wedge parameter on f′(η)

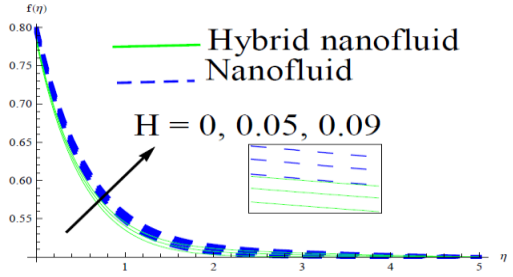

Fig. 3: Effect of magnetic field on f ′(η)

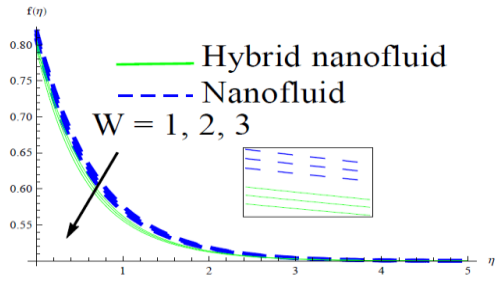

Fig. 4: Effect of Weissenberg number on f ′(η)

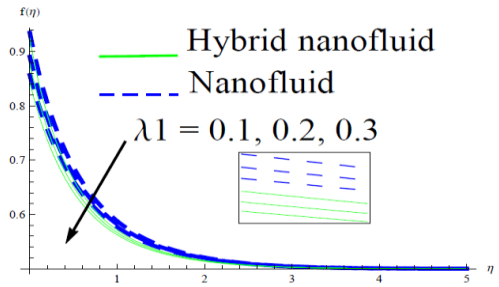

Fig. 5: Behaviour of $\lambda_1$on f ′(η)

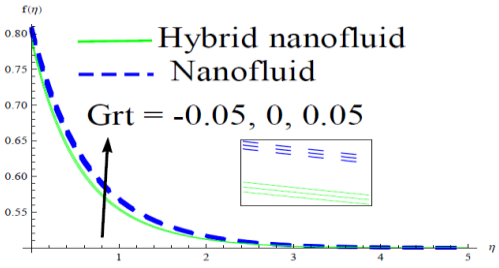

Fig. 6: Influence of Grashof number on f ′(η)

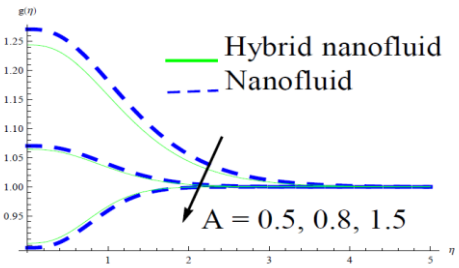

Fig. 7: Effect of stretching parameter on g (η)

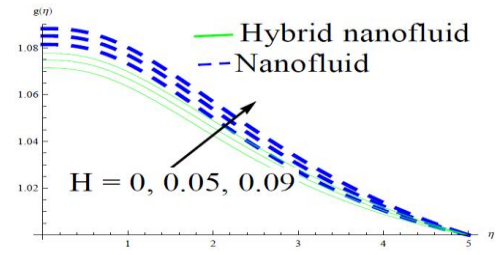

Fig. 8: Variation of magnetic field on g (η)

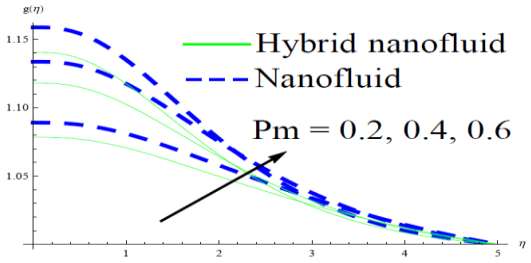

Fig. 9: Impact of Pm against g (η)

It is important to note that internal heat generation occurs when $\alpha > 0$ and $\beta > 0$, while internal heat absorption occurs when $\alpha < 0$ and $\beta < 0$. Across the boundary layer region, the temperature rises or falls depending on the combined impacts of heat source/sink characteristics.

As we can see from Fig. 11 and 12, enhancing the values of $\alpha > 0$ and $\beta > 0$ increases the fluid temperature, while more energy is absorbed when the values of $\alpha < 0$ and $\beta < 0$ escalate, leading to a significant decrease in temperature in the direction of the boundary layer. Furthermore, the heat source's thermal boundary layer is thicker than the heat sink's. With the help of Fig. 13, the impact of ω (thermal slip parameter) is examined. It is observed that increasing ω values cause the profile to drop. As noted by Sabu et al [37], increasing the thermal slip parameter lowers the temperature by reducing the sensitivity of the fluid flow inside the boundary layer. This lowers the quantity of heat generated. The temperature graphs' fluctuation in relation to the radiation parameter Rd is shown in Fig. 14. Temperature and thermal boundary layer thickness increase in tandem with increases in Rd values. The fluid temperature rises in response to an increase in thermal radiation, increasing the thermal boundary layer thickness in the process. This implies that heat radiation automatically increases as Rd increases. From a physical perspective, it is noted that the radiation process raises the temperature of the nanoparticles by producing heat in the working liquid. The temperature graphs' variation with respect to the Eckert parameter Ec is shown in Fig. 15. Temperature and thermal boundary layer thickness grow in tandem with increases in Ec values. The fluid temperature rises with an increase in Ec, leading to a physical increase in the thickness of the thermal boundary layer. This implies that the thermal layer is automatically enlarged when the Eckert parameter is increased. Physically, it is seen that the Ec raises the temperature of the nanoparticles by producing heat in the working liquid.

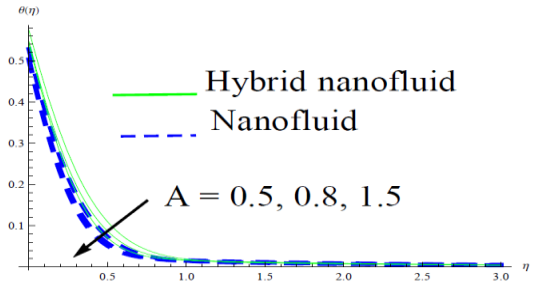

Fig. 10: Impact of stretching parameter on $\theta(\eta)$

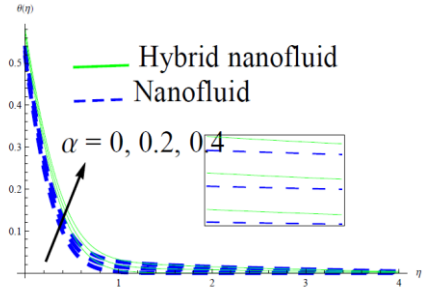

Fig.11 Impact of heat generation/absorption on$\theta(\eta)$

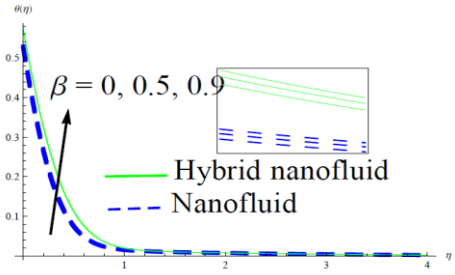

Fig. 12: Effect of heat generation/absorption on$\theta(\eta)$

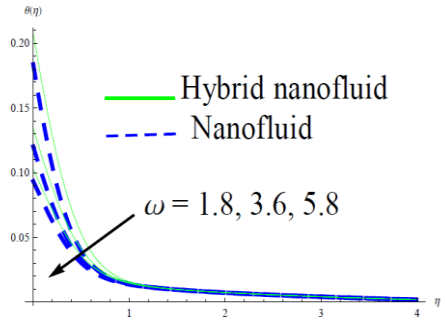

Fig. 13: Effect of thermal slip on $\theta(\eta)$

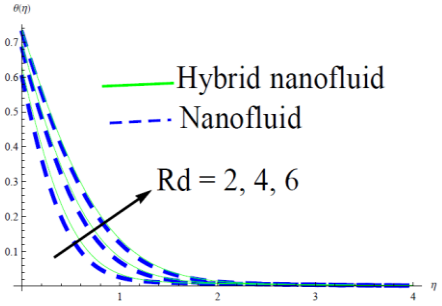

Fig. 14: Radiation effect against$\theta(\eta)$

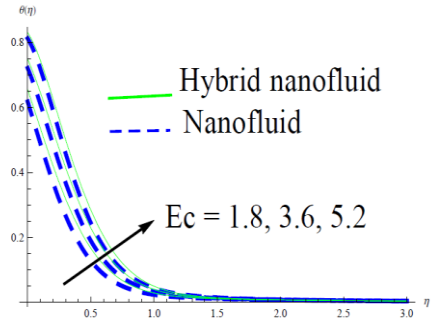

Fig. 15: Eckert number impact on$\theta(\eta)$

IV. CONCLUSION AND OBSERVATION

The present study thoroughly investigates the impacts of various fluid regulating parameters on the behavior of hybrid nanofluid flow over a stretching wedge, using a semi-analytical solution derived from the homotopy analysis method. The results are in strong agreement with previous research conducted by Mohamed & Ahmed [31], Ali et al. [24], Ishak et al. [35], and Mahapatra & Gupta [36], particularly when the variable heat source/sink and magnetic thermal buoyancy are negligible.

Key observations from this study include:

1. Velocity Field:

- The fluid velocity $f'(\eta)$ increases with a higher stretching parameter (A). For $A = 1$, the fluid and wedge surface velocities match, while $A > 1$ enhances fluid velocity, and $A < 1$ reduces it.
- The magnetic parameter (H) positively influences fluid velocity $f'(\eta)$, as does the thermal Grashof number.
- Higher Weissenberg numbers (W) reduce both the hydrodynamic boundary layer strength and fluid velocity.
- Increasing the velocity-slip parameter decreases fluid velocity along the wedge boundary.

2. Induced Magnetic Field:

- The induced magnetic field $g(\eta)$ decreases with higher values of the stretching parameter (A), and increases with the magnetic parameter (H).
- A higher magnetic Prandtl number (Pm) reduces the strength of the induced magnetic field $g(\eta)$.

3. Temperature Field:

- The temperature of the fluid decreases with an increasing stretching parameter (A), with lower temperature profiles for nanofluids compared to hybrid nanofluids.
- Internal heat generation occurs when $\alpha > 0$ and $\beta > 0$, while absorption happens when $\alpha < 0$ and $\beta < 0$, influencing the boundary layer temperature accordingly.
- Increasing values of $\alpha > 0$ and $\beta > 0$ raise fluid temperature, whereas $\alpha < 0$ and $\beta < 0$ significantly decrease it.
- The thermal slip parameter (ω) reduces fluid temperature, while the radiation parameter (Rd) and Eckert parameter (Ec) both increase the temperature and thermal boundary layer thickness.

These findings as illustrated through Figs. 2-15 and Tables 4 and 5, confirming that the semi-analytical solution closely aligns with the numerical solutions for various parameter values. The comprehensive analysis underscores the significant role of fluid regulating parameters in determining the flow and thermal characteristics of hybrid nanofluids, providing valuable insights for optimizing fluid dynamics in engineering applications.

REFERENCES

[1]. L. J. Crane, "Flow past a stretching plate," Z Angew Math Phys., vol. 21, pp. 645–55, 1970.

[2]. P. Carragher and L. J. Crane, "Heat transfer on a continuous stretching sheet," ZAMM Z Angew Math Mech, vol. 62, pp.564–73, 1982.

[3]. E. Magyari and B. Keller, "Heat and mass transfer in the boundary layers on an exponentially stretching continuous surface," J. Phys D: Appl Phys., vol. 32, pp.577–85, 1999.

[4]. M. K. Partha, P. V. S. N. Murthy, and G. P. Rajasekhar, "Effect of viscous dissipation on the mixed convection heat transfer from an exponentially stretching surface," Heat Mass Transfer, vol. 41, pp. 360–6, 2005.

[5]. B. Bidin and R. Nazar "Numerical solution of the boundary layer flow over an exponentially stretching sheet with thermal radiation," Eur J Sci Res. vol. 33, issue 4, pp. 710–7, 2009.

[6]. A. Ishak, "MHD boundary layer flow due to an exponentially stretching sheet with radiation effect," Sains Malays, vol. 40, pp. 391–5, 2011.

[7]. E. M. A. Elbashbeshy, et al, "Flow and heat transfer over a stretching surface with variable thickness in a Maxwell fluid and porous medium with radiation," vol. 23, issue 5B, pp. 3105-3116, 2019.

[8]. M. N. Tufail, A. Saeed, and A. Ali, "Heat source/sink effects on non-Newtonian MHD fluid flow and heat transfer over a permeable stretching surface," Indian Journal of Physics, vol. 88, issue 1, pp. 75-88, 2013.

[9]. T. Rasheed, T. Hussain, M. T. Anwar, J. Ali, K. Rizwan, M. Bilal, F. H. Alshammari, N. Alwadai, and A. S. Almuslem, A. S. "Hybrid Nanofluids as Renewable and Sustainable Colloidal Suspensions for Potential Photovoltaic/Thermal and Solar Energy Applications," Frontiers in Chemistry, vol. *9*, 737033, 2021, doi.org/10.3389/fchem.2021.737033.

[10]. Z. Shah, A. Saeed, I. Khan, M. M. Selim, and P. Kumam, "Numerical modeling on hybrid nanofluid (Fe_3O_4+MWCNT/H_2O) migration considering MHD effect over a porous cylinder," *PLOS ONE*, vol. *16, issue* 7, 2021, doi:10.1371/journal.pone.0251744.

[11]. T. Hayat, S. Nadeem, and A.U. Khan. "Numerical analysis of Ag–CuO/water rotating hybrid nanofluid with heat generation and absorption," Canadian Journal of Physics, vol. 97, issue 6, pp. 644-650, 2019, doi:10.1139/cjp-2018-0011.

[12]. Muhammad Khairul Anuar Mohamed et al "Heat Transfer of *Ag-Al_2O_3/Water* Hybrid Nanofluid on a Stagnation Point Flow over a Stretching Sheet with Newtonian Heating," *J. Phys.: Conf. Ser.* Vol. 1529 pp. 042-85, 2020.

[13]. P. Sreedevi, P. Sudarsana Reddy, and A. Chamkha, "Heat and mass transfer analysis of unsteady hybrid nanofluid flow over a stretching sheet with thermal radiation," SN Appl. Sci. vol. 2, pp. 12-22, 2020, doi:10.1007/s42452-020-3011-x.

[14]. A. S. Alnahdi, and T. Gul, "Hybrid nanofluid flow over a slippery surface for thermal exploration," Advances in Mechanical Engineering, 2023, doi.org/10.1177/16878132231190060

[15]. G. S. Beavers and D. D. Joseph, "Boundary conditions at a numerically permeable wall," Journal of Mechanics, vol. 30, pp. 197–207, 1967.

[16]. A. A. Afify, M. J. Uddin, and M. Ferdows, "Scaling group transformation for MHD boundary layer fow over permeable stretching sheet in presence of slip fow with Newtonian heating efects," Applied Mathematics and Mechanics-English Edition, vol. 35, issue 11, pp. 1375–1386, 2014.

[17]. J. A. Gbadeyan, J. U. Abubakar, T. L. Oyekunle, "Effects of Navier slip on a steady flow of an incompressible viscous fluid confined within spirally enhanced channel," Journal of the Egyptian Mathematical Society, vol. 28, issue 1, 2020, DOI: 10.1186/s42787-020-00081-9

[18]. A. Aziz, J. I. Siddique, and T. Aziz, "Steady Boundary Layer Slip Flow along with Heat and Mass Transfer over a Flat Porous Plate Embedded in a Porous Medium," *PLOS ONE*, vol. *9*, issue 12, e114544, 2014, doi:10.1371/journal.pone.0114544.

[19]. M. W. Hamza, "Free convection slip flow of an exothermic fluid in a convectively heated vertical channel," Ain Shams Engineering Journal, vol. 9, issue 4, 2018.

[20]. H. I. Andersson, "Slip flow past a stretching surface," Acta Mech, vol. 158, pp. 121–5, 2002.

[21]. Z. Abbas, Y. Wang, T. Hayat, M. Oberlack, "Slip effects and heat transfer analysis in a viscous fluid over an oscillatory stretching surface," Internat. J. Numer. Methods Fluids, vol. 59, pp. 443–58, 2009.

[22]. M. Turkyilmazoglu, "Effects of partial slip on the analytic heat and mass transfer for the incompressible viscous fluid of a porous rotating disk flow," J. Heat Transfer, vol. 33, issue 12, 122602, 2011.

[23]. M. Kumari, H. S. Takhar, G. Nath, "Magneto hydrodynamic flow and heat transfer over a stretching surface with prescribed wall temperature or heat flux," Warme ¨ - Und Stoffübertragung, vol. 25, pp. 331–336, 1990, doi:10.1007/BF01811556.

[24]. F. M. Ali, R. Nazar, N. M. Arifin, I. Pop, "Magneto hydrodynamic boundary layer flow and heat transfer over a stretching sheet with induced magnetic field," Heat Mass Transf. vol. 47, pp. 155–162, 2011, doi.org/10.1007/s00231-010-0693-4.

[25]. T. Hayat, A. Sadia and A. Alsaedi, "Non-Uniform Heat Source/Sink and Thermal Radiation Effects on the Stretched Flow of Cylinder in a Thermally Stratified Medium," Journal of Applied Fluid Mechanics, vol. 10, issue 3, pp. 915-924, 2016, DOI: 10.18869/acadpub.jafm.73.240.24008

[26]. J. R. Konda, N. R. Madhusudhana, R. Konijeti and A. Dasore, "Effect of non-uniform heat source/sink on MHD boundary layer flow and melting heat transfer of Williamson nanofluid in porous medium," Multidiscipline Modeling in Materials and Structures, vol. 15, issue 2, pp. 452-472, 2019, doi:10.1108/MMMS-01-2018-0011.

[27]. B. Manvi, J. Tawade, M. Biradar, S. Noeiaghdam, U. Fernandez-Gamiz, and V. Govindan, "The effects of MHD radiating and non-uniform heat source/sink with heating on the momentum and heat transfer of Eyring-Powell fluid over a stretching," Results in Engineering, vol. *14*, 100435, 2022, doi:10.1016/j.rineng.2022.100435.

[28]. S. K. Rawat, M. Yaseen, U. Khan, M. Kumar, S. M. Eldin, A. M. Alotaibi, and A. M. Galal, "Significance of non-uniform heat source/sink and cattaneo-christov model on hybrid nanofluid flow in a Darcy-forchheimer porous medium between two parallel rotating disks," Frontiers in Materials, vol. *9*, 1097057, 2023.

[29]. K. Mehmood, S. Hussain and M. Sagheer, "Mixed convection flow with non-uniform heat source/sink in a doubly stratified magneto-nanofluid," AIP Advances, vol. 6, 065126, 2016, doi:10.1063/1.4955157.

[30]. A. M. Okedoye and P. O. Ogunniyi, "MHD Boundary Layer flow past a moving plate with mass transfer and Binary Chemical Reaction," Journal of the Nigerian Mathematical Society, vol. 38, issue 1, pp. 89 -121, 2019.

[31]. A. E. Mohamed and A. A. Ahmed, "Influences of Slip Velocity and Induced Magnetic Field on MHD Stagnation-Point Flow and Heat Transfer of Casson Fluid over a Stretching Sheet," Mathematical Problems in Engineering, vol. 2018, Article ID 9402836, pp. 1-11, 2018, doi:10.1155/2018/9402836

[32]. P. O. Ogunniyi**,** J. A. Gbadeyan, M. C. Agarana, T. A. Yusuf, "Nonlinear thermal radiation on MHD tangential hyperbolic hybrid nanofluid over a stretching wedge with convective boundary condition," Heat Transfer, vol. **51**, issue 6, pp. 5417–5440, 2022.

[33]. S. J. Liao, "The proposed homotopy analysis technique for the solution of non-linear problems (Ph.D. thesis)," Shanghai Jiao Tong university; 1992.

[34]. S. J. Liao, "Beyond perturbation: Introduction to homotopy analysis method," Boca Raton: Chapman & Hall/CRC Press, 2003.

[35]. A. Ishak, R. Nazar and I. Pop, "Boundary layer flow of a micropolar fluid on a continuous moving or fixed surface," Canadian Journal of Physics, vol. 84, issue 5, pp. 399-410.

[36]. T. R. Mahapatra and A. S. Gupta, "Heat Transfer in Stagnation point flow towards a stretching sheet," Heat and Mass Transfer, vol. 38, pp. 517-521, 2002.

[37] A. S. Sabu, J. Mackolil, B. Mahanthesh et al, "Reiner-Rivlin nanomaterial heat transfer over a rotating disk with distinct heat source and multiple slip effects," Appl. Math, Mech. Ed., vol. 42, pp. 1495-1510, 2021.